Mean free path spectra as a tool to understand thermal conductivity in bulk and nanostructures

Fan Yang and Chris Dames*
Department of Mechanical Engineering, University of California at Berkeley, California 94720, USA
(Received 18 July 2012; published 31 January 2013)

A rigorous derivation is given for the thermal conductivity accumulation function and mean free path (MFP) spectrum of an isotropic bulk material. The key physical insight is to express the kinetic theory integral in terms of MFP rather than frequency. Extending this framework to incorporate boundary scattering in nanostructures leads to an integral equation that transforms a material's bulk MFP spectrum into the size-dependent thermal conductivity of the nanostructure. The kernel of this transform represents the boundary scattering rule for the particular type of nanostructure. The principal benefit of this transform is that it requires only a single function, the material's bulk MFP spectrum, or equivalently its accumulation function. Explicit knowledge of the material's dispersion relation and frequency-dependent bulk MFPs is not needed, nor is a summation over polarizations, because the bulk MFP spectrum already contains this information in exactly the form required to evaluate boundary scattering. The utility of this framework is demonstrated through a case study of six models for the phonon thermal conductivity of silicon: three analytical, one gray, and two numerical.

DOI: 10.1103/PhysRevB.87.035437 PACS number(s): 44.05.+e, 44.10.+i, 63.22.Gh, 65.80.−g

I. INTRODUCTION

The thermal conductivity of a nanostructured material can be greatly reduced compared to its bulk counterpart due to the increased scattering of energy carriers (e.g., phonons, electrons, photons, gas molecules) at the nanostructure surfaces, as in wires,[1] films,[2,3] porous[4] and nanocrystalline[5] materials, etc. Thermal transport in such nanostructured materials is relevant for a broad range of applications in energy conversion,[6] sensors,[7,8] microelectronics,[9] and lasers.[10] The key physics that determines the importance of this boundary scattering is the comparison between the characteristic length of the nanostructure and the bulk mean free paths (MFPs) of the energy carriers. Thus it is very helpful to have a detailed quantitative understanding of which bulk MFPs are important in a given material.

The most common formulas for the bulk thermal conductivity are based on kinetic theory, which can be derived from the Boltzmann transport equation in the relaxation time approximation.[11,12] The polarization dependence and frequency dependence of the heat capacity, group velocity, and MFPs are readily accounted for using a summation and integration, respectively. Recently, a new perspective expressing the thermal conductivity integral in terms of MFPs rather than frequency has been developed.[13–22] The main benefit of this MFP spectrum approach is that it quantifies the contribution of every MFP to the bulk thermal conductivity. An equivalent concept is the thermal conductivity accumulation function, which is the normalized integral of this MFP spectrum. The resulting distributions visually and intuitively show which ranges of MFPs are most important for thermal conductivity, information which is not readily apparent in the traditional and complementary approach of plotting the MFPs as functions of frequency.

Although the concept of a MFP spectrum applies to heat conduction by all types of energy carriers, most prior work has focused on calculations for phonons, including MFP distributions for analytical models[13,15] and numerical results from molecular dynamics (MD) simulations[14] and first-principles (1stP) calculations based on density functional theory.[12,17,20,21] Measurements of portions of the phonon MFP distribution are also beginning to be reported for silicon[18] and several semiconductor alloys,[19] although analyzing the raw data requires certain assumptions which, although plausible, have not yet been rigorously proven.

Here, we revisit the concept of the bulk MFP spectrum and show how it is also useful for understanding nanostructures. This paper has three major objectives. First, we rigorously rederive the expressions for the bulk MFP distribution and thermal conductivity accumulation function first given by Dames and Chen,[13] identifying the major assumptions and restrictions, not all of which were noted previously. Then we derive an integral transform which, given a bulk MFP distribution and a boundary scattering law, yields the thermal conductivity of a nanostructure as a function of its characteristic length. As summarized in Fig. 1, this integral equation does not require any explicit knowledge of the carrier's dispersion relation or frequency-dependent scattering laws and thus represents a quantitative application of the MFP spectrum beyond its more common use for visualizing MFP distributions. Finally, to demonstrate these concepts we present a detailed case study of the phonon thermal conductivity of bulk and nanostructured silicon, revealing major differences among the MFP spectra of three common analytical models (Callaway,[23] Holland,[24] and Born–von Karman-Slack[13]), an MD simulation,[14] and a 1stP calculation.[20]

II. THEORETICAL FRAMEWORK

A. Bulk MFP spectrum and thermal conductivity accumulation function

Our starting point is the kinetic theory integral for the thermal conductivity of an isotropic bulk material,

$$\kappa_{\text{bulk}} = \sum_s \int_0^\infty \frac{1}{3} C v \Lambda_{\text{bulk}} d\omega, \tag{1}$$

where C is the volumetric specific heat capacity per unit frequency, v is the group velocity, Λ_{bulk} is the bulk MFP, ω is the frequency, and s indexes the polarizations. The

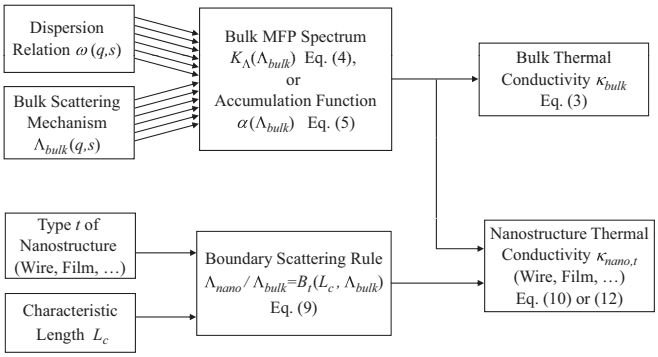

FIG. 1. The framework of using a MFP spectrum (or, equivalently, accumulation function) to model the thermal conductivity of an isotropic bulk material and a corresponding nanostructure. The multiple arrows at top left suggest multiple polarizations s. Other variables are defined in the main text.

most important assumption of this work is that the dispersion relation and bulk MFPs are well-approximated as isotropic. From symmetry considerations this assumption is exact for gases (e.g., molecules, photons, free electrons), as well as electrons and phonons in amorphous materials. In crystalline materials the dispersion relation of electrons and phonons depends on direction and a more general form[12] of Eq. (1) is appropriate, even if κ_{bulk} itself is isotropic (as in crystals with cubic symmetries). Nevertheless, such dispersion anisotropies are commonly neglected in models of the thermal conductivity that have been shown to agree well with experiments in cubic crystals as well as noncubic crystals that are only weakly anisotropic,[23–28] and the present work is limited to materials where this isotropic approximation is acceptable. Furthermore, to ensure that the only subcontinuum effects are due to boundary scattering and not ultrafast phenomena, the analysis is restricted to heat transfer problems that are steady, or if unsteady involve transients that are slow compared to the carrier relaxation times τ.

To focus the theoretical framework on the bulk MFPs, we formally change the integration variable from ω to Λ_{bulk}, obtaining

$$\kappa_{\text{bulk}} = -\sum_s \int_0^\infty \frac{1}{3} C v \Lambda_{\text{bulk}} \left(\frac{d\Lambda_{\text{bulk}}}{d\omega}\right)^{-1} d\Lambda_{\text{bulk}}. \quad (2)$$

The negative sign arises from swapping the limits of integration, because the dominant trend of $d\Lambda_{\text{bulk}}/d\omega$ is negative, and the final value of κ_{bulk} will still be positive.

Physically, the change of variables in Eq. (2) can be understood as changing to a different labeling scheme for the energy carriers. In general, four numbers are required to uniquely specify a carrier, for example, $\{q_x,q_y,q_z,s\}$ or $\{q,\theta,\phi,s\}$, where $\mathbf{q}$ is the wave vector of magnitude q and direction (θ,ϕ). It is common to use the dispersion relation $\omega = \omega(\mathbf{q},s)$ to change the labeling scheme to $\{\omega,\theta,\phi,s\}$. The change of variables in Eq. (2) is equivalent but instead uses the bulk scattering function $\Lambda_{\text{bulk}} = \Lambda_{\text{bulk}}(\mathbf{q},s)$ to get a $\{\Lambda_{\text{bulk}},\theta,\phi,s\}$ scheme. Then, with the key assumption that $\omega(\mathbf{q},s)$ and $\Lambda_{\text{bulk}}(\mathbf{q},s)$ are approximately isotropic, the labeling scheme reduces to simply $\{\Lambda_{\text{bulk}},s\}$. That is, every energy carrier is uniquely identified by its bulk MFP and polarization branch.

For fixed s, often Λ_{bulk} is a smooth, monotonically decreasing function of ω. In cases where $\Lambda_{\text{bulk}}(\omega,s)$ is not monotonic in ω, the inverting function $\omega(\Lambda_{\text{bulk}},s)$ will be multivalued and there may appear to be an ambiguity in the $\{\Lambda_{\text{bulk}},s\}$ labeling scheme. However, this is easily remedied by breaking the offending polarization branch into piecewise monotonic sections and increasing the number of branches in the index list s accordingly. This remedy of piecewise integration can also be used to avoid any singularities which arise at points where $\frac{d\Lambda_{\text{bulk}}}{d\omega} = 0$.

Returning to Eq. (2), because the integrals converge we apply Fubini's theorem to exchange the orders of summation and integration and write

$$\kappa_{\text{bulk}} = \int_0^\infty K_\Lambda d\Lambda_{\text{bulk}}, \quad (3)$$

where

$$K_\Lambda = -\sum_s \frac{1}{3} C v \Lambda_{\text{bulk}} \left(\frac{d\Lambda_{\text{bulk}}}{d\omega}\right)^{-1} \quad (4)$$

is the thermal conductivity per MFP, with SI units (W/m^2 K). This function[13] is known as the MFP distribution or MFP spectrum for the bulk thermal conductivity. By definition, the quantity $K_\Lambda(\Lambda_{\text{bulk}}) \cdot d\Lambda_{\text{bulk}}$ represents the differential thermal conductivity due to those energy carriers with MFPs between Λ_{bulk} and $\Lambda_{\text{bulk}} + d\Lambda_{\text{bulk}}$.

A complementary perspective is the thermal conductivity accumulation function,

$$\alpha(\Lambda_\alpha) = \frac{1}{\kappa_{\text{bulk}}} \int_0^{\Lambda_\alpha} K_\Lambda d\Lambda_{\text{bulk}}, \quad (5)$$

which represents the fraction of the total thermal conductivity due to carriers with MFPs less than Λ_α. Thus, the range $\Lambda_{0.1} < \Lambda_{\text{bulk}} < \Lambda_{0.9}$, analogous to the 10%–90% rise time of a signal on an oscilloscope, is one useful guideline to the range of bulk MFPs that are important for heat conduction in a given system: 80% of the thermal conductivity is carried by particles with MFPs in this range, with only 10% carried by MFPs shorter than $\Lambda_{0.1}$ and another 10% carried by MFPs longer than $\Lambda_{0.9}$.

Equations (4) and (5) are the first major results of this paper. These equations quantify the range of MFPs that contribute to heat conduction, which traditionally was described mainly through a single lumped "gray" or effective MFP,

$$\Lambda_{\text{gray}} = \kappa_{\text{bulk}} \Big/ \left(\sum_s \int_0^\infty \frac{1}{3} C v d\omega\right). \quad (6)$$

This is equivalent to a MFP distribution that is a Dirac δ function with weight κ_{bulk} centered on Λ_{gray}. Such a gray MFP model is a good approximation in systems where the real MFP distribution is narrow, including ideal gases[29] and free electron gases. However, in other systems with strongly frequency-dependent scattering, the distributions can be quite broad. For example, as we discuss further in Sec. III, phonons in semiconductor crystals and alloys are generally believed to have MFP distributions typically spanning two or more orders of magnitude from $\Lambda_{0.1}$ to $\Lambda_{0.9}$.[13–15,18–21]

B. An integral transform to relate bulk and nanostructures

We now shift attention from bulk to nanostructures and make the common assumption that wave confinement effects are negligible. This is generally appropriate as long as the structure's characteristic length L_c is much larger than the thermal wavelengths of the energy carriers[13,30,31] and there is sufficient roughness or disorder to wash out any coherence effects. Thus, the group velocity and spectral heat capacity in the nanostructure are identical to those in bulk, so the only effect of the nanostructuring is to reduce the effective MFP Λ_{nano} by scattering at boundaries and interfaces. Thus, the nanostructure thermal conductivity is commonly written[3,5,13,32,33]

$$\kappa_{\text{nano},t} = \sum_s \int_0^\infty \frac{1}{3} C v \Lambda_{\text{nano}} d\omega, \tag{7}$$

where $\Lambda_{\text{nano}}(\omega,s) < \Lambda_{\text{bulk}}(\omega,s)$ and the subscript t indicates the "type" of geometry (such as a wire, film, etc.). We again change variables from ω to Λ_{bulk} and rearrange to obtain

$$\kappa_{\text{nano},t} = \int_0^\infty \left[-\sum_s \frac{1}{3} C v \Lambda_{\text{bulk}} \left(\frac{d\Lambda_{\text{bulk}}}{d\omega} \right)^{-1} \right] \frac{\Lambda_{\text{nano}}}{\Lambda_{\text{bulk}}} d\Lambda_{\text{bulk}}, \tag{8}$$

where the term in square brackets is exactly the bulk MFP spectrum K_Λ from Eq. (4), an important feature we return to shortly. Recall that physically this change of variables from ω to Λ_{bulk} is equivalent to choosing to label each carrier by its polarization and *bulk* MFP, even though now that carrier's MFP in the nanostructure is reduced to Λ_{nano}.

There is a deep physical reason for choosing Λ_{bulk} as the independent variable in Eq. (8), rather than τ_{bulk}, ω, q, wavelength λ, or indeed any other quantity. The key is in the functional dependencies of the effective MFP Λ_{nano}. Λ_{nano} obviously must depend on L_c and the type of nanostructure (wire, film, etc.). More importantly, we recognize the very general result that Λ_{nano} transitions between bulk and strongly confined behaviors depending primarily on the comparison between L_c and Λ_{bulk}. Therefore, the simplest, and also very common, situation is that Λ_{nano} is a function exclusively of L_c and Λ_{bulk}. In this case, from basic considerations of dimensional analysis the functional relationship between these three length scales must be expressible in the form

$$\frac{\Lambda_{\text{nano}}}{\Lambda_{\text{bulk}}} = B_t \left(\frac{\Lambda_{\text{bulk}}}{L_c} \right) = B_t \left(\text{Kn} \right). \tag{9}$$

Here B_t is some function to be determined that depends only on the type of nanostructure and on the *ratio* $\Lambda_{\text{bulk}}/L_c$. Note that this reasoning has nothing to do with Matthiessen's rule and that the ratio $\Lambda_{\text{bulk}}/L_c$ is the Knudsen number, Kn.

Thus, of all possible quantities to label an energy carrier, it is uniquely Λ_{bulk} that has the strongest physical connection to the processes of boundary scattering. Indeed, for a wide variety of geometries the most common boundary scattering laws for Λ_{nano} can be written in the form of Eq. (9) without any other explicit dependence on polarization, group velocity, frequency, etc. Examples include wires of arbitrary cross section,[34–36] thin films both in-plane and cross-plane,[37–40] porous media with arbitrary pore shapes and distributions,[15] and simple models of grain boundary scattering.[5,41,42] Equation (9) will also result for the combined effect of scattering by bulk and surface mechanisms in single-phase structures with arbitrarily complicated geometries and with surface roughness, as long as all of the important energy carriers experience the same specularity, p, representing the probability of specular scattering.[43] Such a constant p approximation has been used for wires[43] and thin films.[37,38]

The most common breakdown of the functional form of Eq. (9) is when p varies substantially with the wavelength of the important energy carriers, as in the transition between specular and diffuse scattering for a surface of roughness δ comparable to the thermal wavelengths.[5,43,44] In this case Eq. (9) could be generalized to $B_t(\text{Kn}, \frac{\lambda}{\delta})$, although such scattering laws would no longer be compatible with the analysis in the remainder of this section. If δ is either much smaller or much greater than the thermal wavelengths, then p should be a constant for all important energy carriers, the wave nature again should be negligible, and the form of Eq. (9) recovered.

Proceeding, we restrict the analysis to those many systems whose boundary scattering laws can be expressed in the form of Eq. (9) and assume that the function $B_t(\text{Kn})$ is known. In this case the nanostructure thermal conductivity in Eq. (8) becomes

$$\kappa_{\text{nano},t} = \int_0^\infty K_\Lambda B_t d\Lambda_{\text{bulk}}. \tag{10}$$

Equation (10) has a counterpart in terms of the accumulation function. Integrating Eq. (10) by parts and using Eq. (5) gives

$$\kappa_{\text{nano},t} = \kappa_{\text{bulk}} [\alpha(\Lambda_{\text{bulk}}) B_t]_{\Lambda_{\text{bulk}}=0}^{\Lambda_{\text{bulk}}=\infty} - \kappa_{\text{bulk}} \int_{\Lambda_{\text{bulk}}=0}^{\Lambda_{\text{bulk}}=\infty} \alpha(\Lambda_{\text{bulk}}) dB_t. \tag{11}$$

From the definition of accumulation, $\alpha(\Lambda_{\text{bulk}}) = 0$ when $\Lambda_{\text{bulk}} = 0$. Furthermore, $B_t \to 0$ as $\Lambda_{\text{bulk}} \to \infty$ because in this limit boundary scattering always dominates regardless of the type of geometry, causing $\Lambda_{\text{nano}} \ll \Lambda_{\text{bulk}}$. Thus, Eq. (11) simplifies to

$$\kappa_{\text{nano},t} = -\kappa_{\text{bulk}} \int_0^\infty \alpha\left(\Lambda_{\text{bulk}}\right) \frac{dB_t}{d\Lambda_{\text{bulk}}} d\Lambda_{\text{bulk}}. \tag{12}$$

As noted above, in the present work the boundary scattering function $B_t(\Lambda_{\text{bulk}}, L_c)$ is considered known,[5,34,36,37] with two specific examples given later in Secs. III C and III D for a wire and film, respectively. As with Eq. (2), the negative sign in Eq. (12) will be cancelled because the dominant trend of $B_t(\Lambda_{\text{bulk}})$ at constant L_c must be of negative $\frac{dB_t}{d\Lambda_{\text{bulk}}}$. Two examples of this trend are shown in Fig. 2 for the simple cases of heat conduction along a round wire and in the plane of a film. The exact expressions used for B_t are given later in Eqs. (16) and (17). To obtain a consistent nondimensional representation of $\frac{dB_t}{d\Lambda_{\text{bulk}}}$ we normalize Λ_{bulk} in the denominator by L_c, yielding $\frac{dB_t}{d\text{Kn}}$. In the limit of very large structures, $L_c \gg \Lambda_{\text{bulk}}$, it is obvious that boundary scattering is negligible and thus $\Lambda_{\text{nano}} \to \Lambda_{\text{bulk}}$, so $B_t \to 1$. Conversely, in the limit of very strong boundary scattering, $L_c \ll \Lambda_{\text{bulk}}$, clearly $\Lambda_{\text{nano}} \ll \Lambda_{\text{bulk}}$ and thus B_t must asymptote towards zero. Therefore, B_t very generally decreases from 1 to 0 with

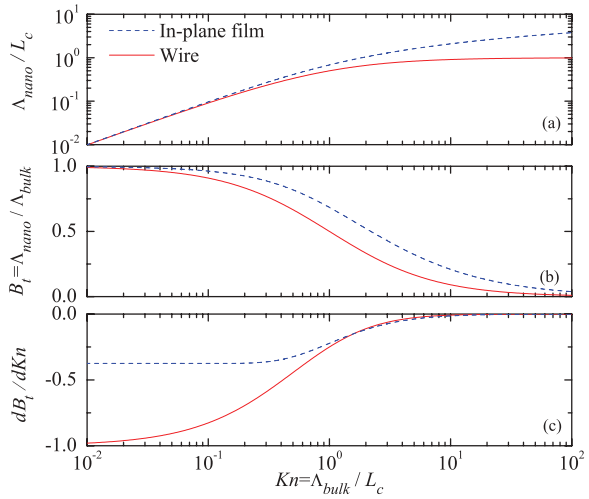

FIG. 2. (Color online) Two examples of the effect of Knudsen number on (a) Λ_{nano}, (b) the integral transform kernel B_t, and (c) its derivative $\frac{dB_t}{d\Lambda_{\text{bulk}}}$. Quantities are nondimensionalized by the nanostructure's characteristic length L_c, taken as the nanowire diameter and film thickness, both of which are assumed diffuse.

increasing Λ_{bulk}, confirming that the dominant behavior of $\frac{dB_t}{d\Lambda_{\text{bulk}}}$ is negative.

Equations (10) and (12) are the second major result of this paper. We recognize both as Fredholm integral equations of the first kind. Equation (10) transforms the bulk MFP spectrum $K_\Lambda(\Lambda_{\text{bulk}})$ to the size-dependent nanostructure conductivity $\kappa_{\text{nano},t}(L_c)$ by means of the kernel B_t. Similarly, Eq. (12) transforms the bulk accumulation function $\alpha(\Lambda_{\text{bulk}})$ to $\kappa_{\text{nano},t}(L_c)$ using the kernel $\frac{dB_t}{d\Lambda_{\text{bulk}}}$.

The flowchart in Fig. 1 summarizes this approach. We emphasize that the theoretical development so far is general and applies to all types of energy carriers, provided their bulk dispersion relations and bulk MFPs are approximately isotropic. As a concrete example of the utility of this approach, consider the phonon thermal conductivity of silicon. For bulk silicon some of the most accurate models are based on 1stP calculations[12,20,21] or MD simulations[14] and thus lack any compact analytical form. After making the isotropic approximation, the traditional way to extend such models to predict the thermal conductivity of, for example, a nanowire is based on Eq. (7). This requires detailed numerical information about 12 functions from the bulk model: the 6 dispersion branches $\omega(q,s)$ and 6 scattering laws $\Lambda_{\text{bulk}}(\omega,s)$. Here the key advantage of writing the kinetic theory integral in terms of MFPs rather than ω becomes apparent: As shown in Fig. 1, Eq. (10) or (12) requires only a *single* numerical function from the bulk model, namely its MFP spectrum K_Λ or, equivalently, its accumulation function α. The information from the six dispersion branches and six scattering laws is not lost, but rather is collapsed into the bulk MFP spectrum [recall Eq. (4)] in exactly the form needed for the nanostructure calculation. Thus, if we can obtain the MFP spectrum or accumulation function of a bulk material—whether from an analytical solution,[13,15] numerical model,[12,14,17,20,21] or experiments[18,19]—given any boundary scattering law Eq. (9) we can also evaluate the thermal conductivity of the corresponding nanostructure.

C. Comparison of MFP spectrum and accumulation function approaches

We have seen that K_Λ and α are both equally valid for visualizing a bulk MFP spectrum as well as transforming it to a nanostructure's thermal conductivity using Eq. (10) or (12). However, there are certain practical reasons to prefer α and Eq. (12). First, for distributions that span more than one order of magnitude in Λ_{bulk}, the accumulation function is far more convenient for visualizing the breadth of the distribution because the ordinate is expressed directly as a fraction of the total thermal conductivity. On the other hand, plots of K_Λ require mentally integrating the area under the curve, which is prone to misunderstanding if a logarithmic abscissa axis is required to cover a large range of Λ_{bulk}.

The second reason why Eq. (12) may be preferred is related to numerical accuracy. Note that Eq. (12) involves the integral of K_Λ (namely, α) and the derivative of B_t, while Eq. (10) involves the derivative of α (namely, K_Λ) and the integral of $\frac{dB_t}{d\Lambda_{\text{bulk}}}$. Note also that the current numerical formulations[14,15,17,20,21] and experimental estimates[18,19] of the MFP distribution arise most fundamentally from an accumulation perspective, $\alpha(\Lambda_{\text{bulk}})$, and thus the numerical differentiation to generate K_Λ is expected to introduce some numerical noise. On the other hand, the expressions for B_t are always analytical, so generating $\frac{dB_t}{d\Lambda_{\text{bulk}}}$ should not introduce any additional noise. Therefore, for numerical reasons the form of Eq. (12) is expected to be preferable to Eq. (10).

D. Gray approximation

The gray model is a common simple approximation where at any given temperature the bulk MFPs are all assumed to take the same gray value, Λ_{gr}. Thus, the thermal conductivity spectrum is a δ function, $K_\Lambda = \kappa_{\text{bulk}}\delta(\Lambda_{\text{bulk}} - \Lambda_{\text{gr}})$, and the accumulation function α is a Heaviside step function, $\alpha = H(\Lambda_{\text{bulk}} - \Lambda_{\text{gr}})$. Applying either Eq. (10) or Eq. (12) shows that this leads to the nanostructure thermal conductivity,

$$\kappa_{\text{nano,gr}} = \kappa_{\text{bulk}} B_t\left(\frac{\Lambda_{\text{gr}}}{L_c}\right) = \kappa_{\text{bulk}} B_t(\text{Kn}_{\text{gr}}), \tag{13}$$

where Kn_{gr} is the Knudsen number of the gray medium.

III. CASE STUDY: PHONONS IN Si

In this section we apply the above concepts to interpret six models of the phonon thermal conductivity of silicon: three analytical, one MD,[14] one 1stP,[20] and a simple gray model for comparison. For the analytical models we use three of the most common: Callaway,[23,27,32,45] Holland,[24] and Born–von Karman-Slack (BvKS).[25,33] Details of our implementation of these models are given in Appendix A, including a modification of the Callaway model with an umklapp scattering law appropriate for all temperatures. Below we present the bulk MFP spectra of these six models and apply the integral transform of Eq. (12) to calculate the corresponding size-dependent thermal conductivity of nanowires and thin films.

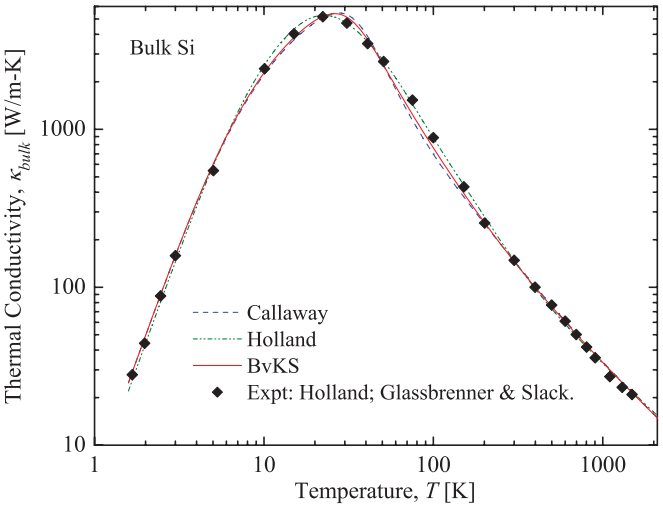

FIG. 3. (Color online) Comparison between three analytical models (lines) and experiment[24,46] (points) for the thermal conductivity of bulk silicon.

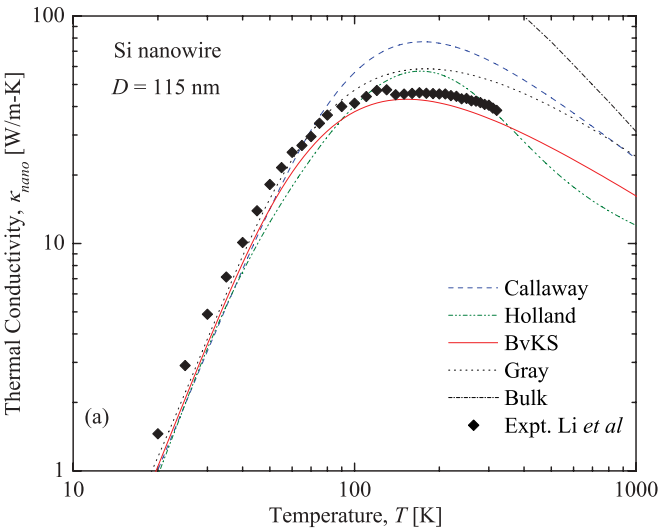

FIG. 4. (Color online) Comparison between models and experiment (Li *et al.*[1]) for the thermal conductivity of a silicon nanowire of diameter 115 nm. The bulk data are from Refs. 24 and 46.

A. Temperature dependence of bulk and nanowire thermal conductivity

For consistency we optimize the three analytical models to the same experimental data set for bulk silicon, from Holland.[24,46] Thus, the fit parameters for our Holland model are identical to those given in the original work,[24] while the parameters for our Callaway and BvKS models are given in Appendix A. As shown in Fig. 3, the three models all fit the experimental data very well. To quantify this agreement we calculate the relative error between each model (κ_{model}) and experiment (κ_{exp}) in a root-mean-square (rms) sense:

$$\varepsilon = \sqrt{\frac{1}{n}\sum_{i=1}^{n}\left(\frac{\kappa_{\text{model}} - \kappa_{\text{exp}}}{\kappa_{\text{exp}}}\right)^2}, \qquad (14)$$

where n is the number of experimental data points. As shown in Table I, after optimizing their parameters the rms errors of these three bulk models are all less than 10%, very good agreement considering they span 2.5–3 orders of magnitude in κ and T.

Even though these models can be tuned to agree closely with each other and with experiments for bulk, the models' internal physical assumptions about C, v, and Λ_{bulk} can be quite different. This begins to become apparent by comparing the three models' predictions for $\kappa_{\text{nano}}(T)$ of a 115-nm-diameter Si nanowire,[1] which tests the models' assumptions about Λ_{bulk} while leaving C and v unchanged. The calculation combines Eq. (12) with the boundary scattering rule given later in Eq. (16).

As shown in Fig. 4 and summarized in Table I, for this nanowire the BvKS model agrees better with the measurements of Li *et al.*[1] than the gray and other analytical models do. Figure 4 also reveals other insights. For example, for nanowires at T above around 100 K the prediction of the modified Callaway model is substantially higher than that of the other models and the experiments. This is because the Callaway model's Debye dispersion overestimates the average phonon group velocities at moderate and large ω. However, as shown in Fig. 3 the Callaway model still fits $\kappa_{\text{bulk}}(T)$ very well. This is accomplished by using overly small Λ_{bulk} to compensate for the overly large Cv at moderate and high T. This is also evident in the comparison of cutoff MFPs between the BvKS and Callaway models in Table I and is discussed further below. Thus, because at most T the Callaway model results in Λ_{bulk} that are too small, when applied to a nanostructure

TABLE I. Key parameters for the six models of bulk Si. Details for the three analytical models are given in Appendix A. The rms errors refer to the fits in Figs. 3 and 4. The cutoff MFPs are defined in Eq. (5) and are evident graphically in Fig. 6(a). The MD data is from Henry and Chen,[14] the 1stP data were provided by Esfarjani[47] at 300 K using the same methods as Ref. 20, and the gray MFP is calculated from Eq. (6) using a BvK dispersion. rms errors were not evaluated for the MD and 1stP models because their temperature dependence was not available.

	rms errors in $\kappa(T)$, ε (%)		Cutoff MFPs at 300 K, Λ_α (nm)			
	Bulk	115-nm nanowire	$\Lambda_{0.1}$	$\Lambda_{0.5}$	$\Lambda_{0.9}$	Bandwidth $\Lambda_{0.9}/\Lambda_{0.1}$
Callaway (modified)	9.2	50	30.1	134	3530	117
Holland	5.8	20	24.4	343	380	15.6
BvKS	6.5	15	79.3	532	14 000	177
MD			41.6	335	15 700	376
1stP			42.8	547	>6580	>154
Gray	0	23	205	205	205	1

the Callaway model is too insensitive to further reductions in Λ_{nano} by boundary scattering, causing it to overpredict κ_{nano} for a given L_c.

B. Bulk MFP spectra and accumulation functions

To quantify the different models' internal assumptions about Λ_{bulk}, we calculated their bulk MFP spectra and accumulation functions using Eqs. (4) and (5), shown in Figs. 5(a) and 5(b), respectively. For comparison, this figure also shows MFP spectra from MD calculations by Henry and Chen[14] and from 1stP calculations by Esfarjani[47] at 300 K, using the same 1stP method as in Ref. 20 at 277 K. It is clear from Fig. 5(b) that the MFP spectra for several of the models extend far beyond 1 μm, so this broad range is better visualized on the logarithmic MFP scale of Fig. 6 at (a) 300 K and (b) 1000 K. The gray MFPs were calculated using the BvKS model and Eq. (6), yielding $\Lambda_{gr} = 205$ nm at 300 K and 44 nm at 1000 K. This gray MFP at 300 K is consistent with other gray calculations for Si (Refs. 48 and 49), which obtain values in the range from 260 to 300 nm. Figure 6 also shows how the MFP spectra are shifted towards shorter Λ_{bulk} at higher T, consistent with the increase in the phonon population (i.e., $\Lambda_{umklapp} \propto T^{-1}$, for T near and above T_{Debye}.)

Figures 5 and 6 reveal striking differences between the various MFP spectra. The models can be roughly grouped into those with broad distributions and those with tight distributions. The first group comprises the Callaway, BvKS, MD, and 1stP models, whose distributions all span more than two orders of magnitude in "bandwidth" from $\Lambda_{0.1}$ to $\Lambda_{0.9}$ (see also Table I). Within this group the Callaway model places more emphasis than the other models do on short MFPs. An important feature of these models is their "long tails": A substantial portion of the heat in bulk is conducted by MFPs much longer than the gray estimate of 205 nm. Specifically, as summarized in Table II, at 300 K bulk MFPs larger than 1 μm account for 19% of the heat conduction in the Callaway model, 31% in the MD results of Ref. 14, 39% in the BvKS model, and 46% of the heat in 1stP results of Ref. 47. Even bulk MFPs longer than 10 μm may not be completely negligible: The BvKS and MD calculations both attribute 12% of the conduction to such long MFPs. The 1stP distribution likely also would assign over 10% of the heat conduction to MFPs larger than 10 μm, though the exact value of α at 10 μm is not available because that calculation stopped at 6.58 μm (found to correspond to $\Lambda_{0.86}$). If the 1stP calculation for the long-MFP tail is assumed to follow a simple scattering law of the form $\Lambda_{bulk} \propto \omega^{-n}$ with known n, an analytical extrapolation function is available (Appendix B).

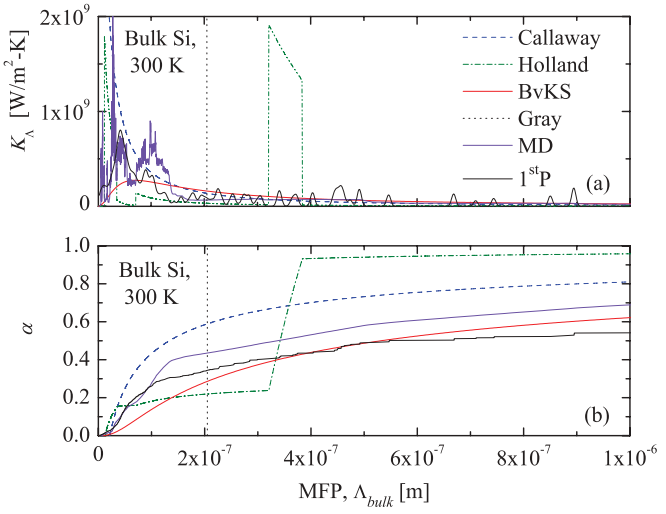

FIG. 5. (Color online) (a) MFP spectra and (b) accumulation functions according to the six models described in the main text. The MD calculation is from Henry and Chen[14] and the 1stP calculation is from Esfarjani *et al.*[20,47]

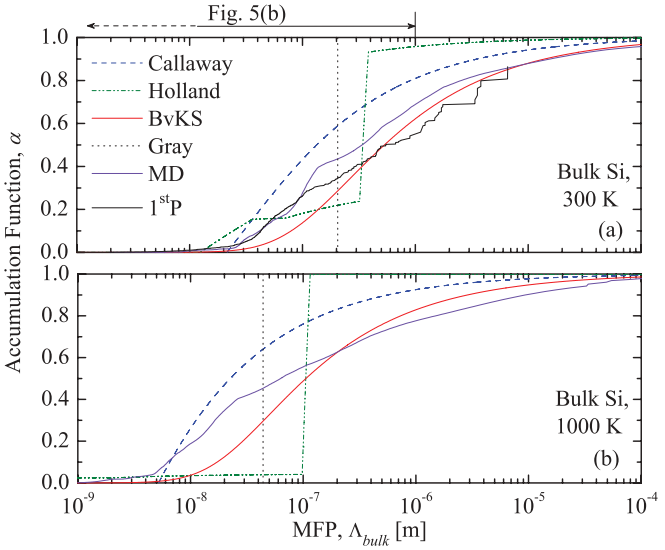

FIG. 6. (Color online) Thermal conductivity accumulation functions for various models at (a) 300 K and (b) 1000 K, using a logarithmic MFP scale. Panel (a) represents a superset of Fig. 5(b). See also Table II. The MD calculation is from Henry and Chen[14] and the 1stP calculation is from Esfarjani *et al.*,[20,47] although the 1stP data were only available at 300 K and $\Lambda_{bulk} \leqslant 6.58$ μm.

The second group of models, with tight distributions, comprises the gray and Holland models. At 300 K in the Holland model of Si over 68% of the heat is carried by high-frequency TA phonons, within the very narrow range of MFPs from 321 to 385 nm. The Holland distribution is even tighter at 1000 K, as shown in Fig. 6(b), with more than 95% of the thermal conductivity contributed by phonons with MFPs from 98 to 116 nm, very much like a gray model.

TABLE II. Fraction of thermal conductivity carried by phonons with MFPs longer than three selected values of Λ_{bulk}, in bulk Si at 300 K. These points are a subset of Fig. 6(a). N/A, not available.

	$1-\alpha(\Lambda_{bulk})$ (%)		
Model	$\Lambda_{bulk} = 0.1$ μm	$\Lambda_{bulk} = 1$ μm	$\Lambda_{bulk} = 10$ μm
Callaway (modified)	57	19	5.8
Holland	82	5.6	2.3
BvKS	86	39	12
MD	72	31	12
1stP	74	46	N/A
Gray	100	0	0

Among all six models presented here, considering their greater sophistication it is reasonable to expect that the MD[14] and 1stP[20,47] models should be the best approximations of real Si. It is noteworthy that these two accumulation functions are also consistent with results from another first-principles calculation recently reported by Li *et al.*,[21] which found $\Lambda_{0.1} =$ 50 nm and $\Lambda_{0.9} = 13\,000$ nm for Si at 300 K. Among the other four models presented here, Tables I and II and Figs. 5 and 6 show that the BvKS results are closest to those from the MD and 1stP calculations, suggesting that among simple models the BvKS model should be more accurate than the gray, Holland, and modified Callaway models.

C. Diameter dependence of thermal conductivity for a nanowire

We now use the integral transform of Eq. (12) to calculate the thermal conductivity of nanowires according to the various bulk accumulation functions presented above in Fig 6(a). For the geometry function B_{wire}, the exact analytical solution of the Boltzmann transport equation in the relaxation time approximation has been given by Dingle.[36] Dingle's result indeed is of the form of Eq. (9), making it appropriate for this framework, but here for convenience we use a more compact analytical expression for a diffuse cylindrical wire based on Matthiessen's rule,

$$\Lambda_{\text{nano}}^{-1} = \Lambda_{\text{bulk}}^{-1} + D^{-1}. \tag{15}$$

It is readily shown that the errors in this approximation are never more than 6% compared to the exact result from Dingle.[36] Thus, for a diffuse nanowire Eq. (9) becomes

$$B_{\text{wire}}(\text{Kn}) = (1 + \text{Kn})^{-1}, \tag{16}$$

where the Knudsen number is $\text{Kn} = \Lambda_{\text{bulk}}/D$.

Although the nanowire thermal conductivity for the gray and analytical (Holland, BvKS, and modified Callaway) models could readily be calculated using the traditional integral over frequency, Eq. (7), here we use the integral transform, Eq. (12). As is suggested in Fig. 1, we emphasize that the traditional approach of Eq. (7) requires knowledge of 12 functions from the bulk model (6 dispersion relations + 6 MFP functions, although the contribution of the optical modes' 3 + 3 functions is often negligible). On the other hand, the strength of Eq. (12) is that it requires only one function (the accumulation function, or equivalently the MFP spectrum), and thus we can proceed without any explicit knowledge of the dispersion relation or frequency-dependent MFPs that are built into the MD[14] or 1stP results[20,47] for α.

Figure 7 shows the calculated nanowire thermal conductivities at 300 K, normalized to the bulk thermal conductivity of 148 W/m K.[24] The accumulation function from Esfarjani *et al.*[20,47] was only available for MFPs $\leqslant 6.58$ μm, at which point $\alpha = 0.86$, whereas Eq. (12) requires integration out to $\Lambda_{\text{bulk}} = \infty$. Therefore, we evaluated $\kappa_{\text{nano}}(D)$ for both bounding limits, where for all $\Lambda_{\text{bulk}} > 6.58$ μm α either jumps immediately to 1 or remains constant at 0.86. For clarity, Fig. 7 shows only the average of these two bounds. For this 1stP result, the difference between the plotted curve and either bound is less than 0.8% of κ_{bulk} for all $D \leqslant 1$ μm, and never exceeds 7% even for $D \to \infty$.

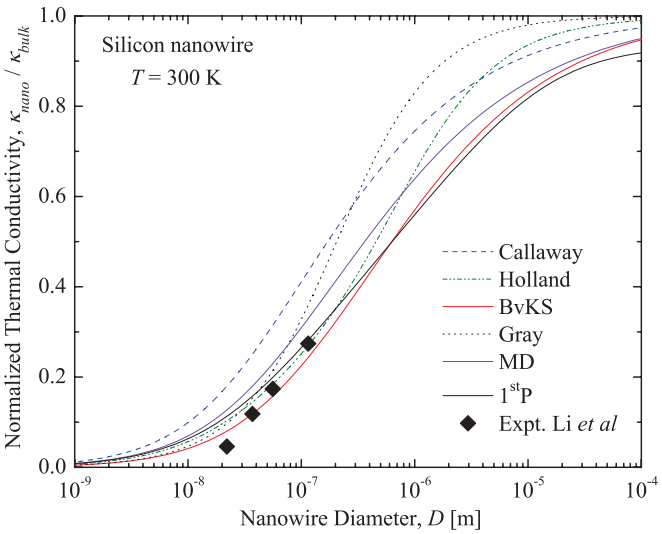

FIG. 7. (Color online) Normalized thermal conductivity $\kappa_{\text{nano}}(D)/\kappa_{\text{bulk}}$ of silicon nanowires calculated using the integral transform of Eq. (12) and assuming diffuse boundary scattering. See also Table III. The experimental data are from Li *et al.*[1] As explained in the main text, the curve for the 1stP spectrum is an average of two bounding cases, with spread less than $\pm 0.8\%$ of κ_{bulk} for $D \leqslant 1$ μm.

Figure 7 also shows that the transition from bulk to strong boundary scattering behavior spans a larger range of D for the Callaway, BvKS, MD, and 1stP models, as compared to the other two models. This is because these four models all have similarly broad accumulation functions as seen from Table I and Fig. 5. The Callaway curve in Fig. 7 is shifted to smaller D than the BvKS, MD, and 1stP calculations, because the Callaway model places more emphasis on shorter MFPs (Figs. 5 and 6). On the other hand, the Holland and gray models show a steeper transition from bulk to confined behavior, because both have much tighter MFP distributions than the other four models.

Table III highlights the differences among the models' predicted thermal conductivity reductions at three selected diameters. For example, at $D = 10$ μm the BvKS model predicts a reduction (17%) that is comparable to that of the MD (15%) and 1stP ($18.2 \pm 4.0\%$) calculations, because these three

TABLE III. Thermal conductivity reduction of silicon nanowires at 300 K compared with bulk, at three selected diameters. These points are a subset of Fig. 7. The range of values for the 1stP calculation reflects extreme bounds due to lack of information for α beyond $\Lambda_{\text{bulk}} = 6.58$ μm (see text).

	Reduction compared to bulk, $(\kappa_{\text{bulk}} - \kappa_{\text{nano}})/\kappa_{\text{bulk}}$ (%)		
Model	$D = 0.1$ μm	$D = 1$ μm	$D = 10$ μm
Callaway (modified)	59	25	9
Holland	75	36	6
BvKS	77	43	17
MD	69	36	15
1stP	73.5 ± 0.1	44.0 ± 0.8	18.2 ± 4.0
Gray	67	17	2

models all have the "longest tails" in their MFP distributions [Fig. 6(a)]. On the other hand, at this same diameter the gray (2%) and Holland (6%) models predict substantially smaller thermal conductivity reductions, because of their tighter MFP distributions and emphasis on shorter bulk MFPs.

Comparing the model curves in Fig. 7 with the experiments of Li *et al.*[1] suggests that the modified Callaway model is not among the top choices. However, additional measurements of larger-diameter samples (e.g., $D = 1$–100 μm) would be needed to discriminate among the other five models. Also, none of these models can explain the measurement of the smallest diameter sample (22 nm), nor other recent reports of sub-Casimir thermal conductivity in Si nanowires.[50–52] Assuming that the MD and 1stP models are most likely to be correct for all diameters, inspection of Fig. 7 and Table III again suggests that among the four simpler models the BvKS model is likely to be most accurate.

D. Thickness dependence of in-plane thermal conductivity for a film

As a second application of the integral transform of Eq. (12), we consider the in-plane thermal conductivity of a film of thickness d and diffuse surfaces. We again emphasize that this calculation uses only the geometry function and accumulation function for each model and does not require explicit knowledge of any dispersion relation or scattering rule $\Lambda_{\text{bulk}}(\omega,s)$. The geometry function B_{film} for this problem is readily obtained from the well-known solution of the Boltzmann transport equation by Fuchs and Sondheimer,[37,38]

$$B_{\text{film}}(\text{Kn}) = 1 - \tfrac{3}{8}\text{Kn}[1 - 4E_3(\text{Kn}^{-1}) + 4E_5(\text{Kn}^{-1})], \tag{17}$$

where E_n is the nth-order exponential integral and here $\text{Kn} = \Lambda_{\text{bulk}}/d$.

The resulting thickness dependence of the film thermal conductivity is shown in Fig. 8. Because of the scatter in the experimental data,[3,48,53] it is not possible to assess which of the models is best. Comparing the models to each other, the major trends are all qualitatively similar to those for the nanowire calculation in Fig. 7. For example, the Holland and gray models again show a sharper transition in $\kappa_{\text{nano}}(D)$, due to their narrower distributions and emphasis on shorter MFPs. Figure 8 also shows the importance of long MFP phonons in the BvKS, MD, and 1stP models: For a 10-μm-thick film, the thermal conductivity reductions compared to bulk are 11% for BvKS, 10% for MD, and 13 ± 5% for 1stP (bounding scenarios), but only 6% for Callaway, 3% for Holland, and less than 1% for the gray model.

E. Broadening of κ_{nano} compared to α

Comparison of Fig. 6(a) with Figs. 7 and 8 suggests that the integral transform of Eq. (12) makes the $\kappa_{\text{nano}}(L_c)$ function even broader than the $\alpha(\Lambda_{\text{bulk}})$ function. This is fundamentally due to the smoothing effect of the kernel,[54] whether $\frac{dB_t}{d\Lambda_{\text{bulk}}}$ [Eq. (12)] or B_t [Eq. (10)]. Focusing on the nanowire example, this broadening effect is more clearly seen in Fig. 9, which plots the accumulation functions and normalized conductivities together on the same axes. We show the BvKS model as a representative of the family of broad-spectrum models (which includes Callaway, MD, and 1stP), and the gray model as a representative of the narrow-spectrum models (the other being Holland). In close analogy to the definition of the cutoff MFPs Λ_α in Eq. (5), here we define cutoff diameters D_β such that

$$\beta(D_\beta) = \frac{\kappa_{\text{nano}}(D_\beta)}{\kappa_{\text{bulk}}}. \tag{18}$$

For example, at $D = D_{0.9}$, the nanowire thermal conductivity is reduced by 10% compared to bulk. For the BvKS model of Si nanowires at 300 K, these cutoff diameters are $D_{0.1} = 30$ nm and $D_{0.9} = 29\,900$ nm, with a "bandwidth" of $D_{0.9}/D_{0.1} = 997$, over five times larger than the MFP bandwidth of $\Lambda_{0.9}/\Lambda_{0.1} = 177$ (Table I). For the gray model, the cutoff diameters are $D_{0.1} = 24$ nm and $D_{0.9} = 1890$ nm, with a bandwidth of $D_{0.9}/D_{0.1} = 79$. Clearly, this represents a great deal of broadening as compared to the gray model's δ-function MFP spectrum ($\Lambda_{0.9}/\Lambda_{0.1} = 1$). A similar broadening effect was also reported in a 1stP calculation for silicon and diamond nanowires.[21]

This broadening effect is relevant for current experimental efforts to measure the MFP distribution,[18,19] which use a plausible though currently unproven postulate that a sharp cutoff condition can be used to estimate a MFP spectrum from the raw measurements. Although those experiments[18,19] are based on unsteady heating with varying frequency, here we consider the analogous postulate for a steady-state problem with varying L_c. Consider a hypothetical siliconlike material with a gray MFP spectrum. As shown in Fig. 9, a set of size-dependent measurements of this material would be broadened to a bandwidth of $D_{0.9}/D_{0.1} = 79$. If this $\kappa_{\text{nano}}(D)$ dataset were then analyzed with a Koh and Cahill-type cutoff condition,[18,19] the estimated MFP spectrum would then also be broadened to $\Lambda_{0.9}/\Lambda_{0.1} = 79$, much larger than the true breadth $\Lambda_{0.9}/\Lambda_{0.1} = 1$. A more sophisticated approach to estimating $\alpha(\Lambda_{\text{bulk}})$ from $\kappa_{\text{nano}}(D)$ would require careful use of

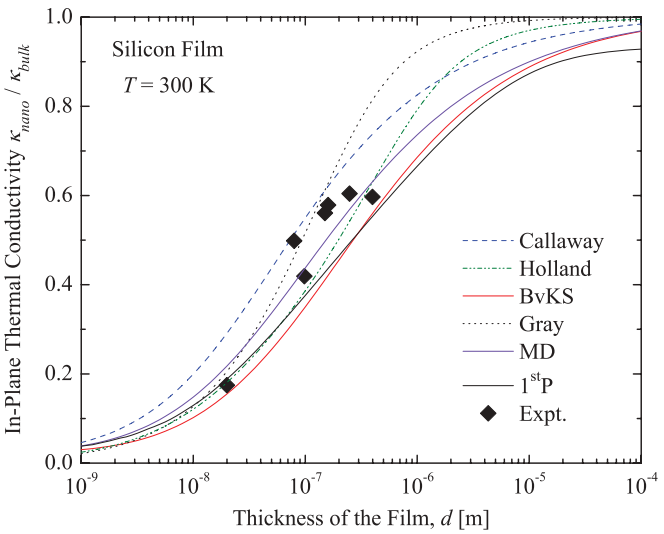

FIG. 8. (Color online) Normalized in-plane thermal conductivity $\kappa_{\text{nano}}(d)/\kappa_{\text{bulk}}$ of silicon thin films, using the integral transform of Eq. (12) and assuming diffuse boundary scattering. The experimental data are from Refs. 3,48, and 53. As with Fig. 7, the result for the 1stP spectrum is an average of two bounding cases.

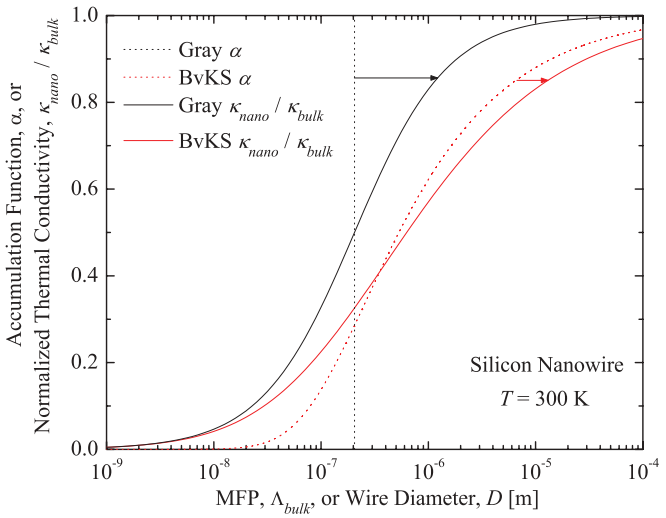

FIG. 9. (Color online) Comparison of the bulk accumulation function (dashed lines) and normalized nanowire thermal conductivity (solid lines) for gray (black) and BvKS (red) models. As indicated by the arrows, for both models the $\kappa_{\text{nano}}(D)$ curves are substantially broadened as compared to the $\alpha(\Lambda_{\text{bulk}})$ curves.

inverse methods,[22] although this is known to be challenging for Fredholm equations of the first kind with smoothing kernels, such as Eqs. (10) and (12).[54]

IV. SUMMARY AND CONCLUSIONS

Expressions for the bulk MFP spectrum [Eq. (4)] and accumulation function [Eq. (5)] have been rigorously rederived.[13] The key physical insight is to write the kinetic theory integral in terms of MFP rather than frequency. The major restrictions are the assumptions that wave confinement effects are negligible, the bulk dispersion relation and bulk MFPs are approximately isotropic, and any thermal transients are much slower than the carrier relaxation times.

Extending this framework to nanostructures leads to the integral transform of Eq. (10). The inputs to the transform are the bulk MFP spectrum and a geometry function for boundary scattering, and the output is the size-dependent thermal conductivity of the nanostructure. Equation (12) is an equivalent transform in terms of the accumulation function, which may be preferred for practical reasons. The most important feature of these transforms is that they require no summation over polarizations and no explicit knowledge of the energy carriers' dispersion relation or bulk scattering rules. Rather, the derivation shows that this information is already incorporated in the bulk MFP spectrum in exactly the form needed to evaluate the additional effects of boundary scattering. This major simplification is not possible if the integrals are expressed in terms of other common quantities such as frequency, wavelength, or relaxation time.

Thus, the framework of MFP spectra (or accumulation functions) has two major benefits: visualization of the important MFPs for bulk thermal conductivity and quantitative evaluation of a nanostructure's thermal conductivity given its bulk MFP spectrum. Therefore, it is hoped that future models of the bulk thermal conductivity will include at least one plot of the accumulation function.[13–21]

To demonstrate these benefits, this paper closes with a case study of six models for phonons in bulk silicon: three analytical,[23–25] one gray, and two purely numerical.[14,20] Among the four simple models, the BvKS model is in closest agreement with the more sophisticated numerical results of Henry and Chen,[14] Li *et al.*,[21] and Esfarjani *et al.*[20,47] This suggests that the BvKS model should be preferred over the gray, Holland, and modified Callaway models for studies involving phonon boundary scattering.[5,13,25] However, further experimental studies of the MFP spectra,[18,19] coupled with rigorous theoretical interpretation, are also needed.

ACKNOWLEDGMENTS

The authors thank Asegun Henry and Keivan Esfarjani for sharing each of their MFP spectra and David G. Cahill and Jonathan A. Malen for sharing their respective analytical results, which form the basis of Appendix B. This work is supported in part by an NSF CAREER award (Grant No. CBET 1055317) and by the DARPA/DSO NMP program (W911NF-08-C-0058).

APPENDIX A: MODELS OF Si THERMAL CONDUCTIVITY

Table IV summarizes the dispersion relations and scattering rules for the three analytical models used in the main text. These models ignore heat conduction by optical phonons and use simple functions to approximate the phonon dispersion and scattering rules for acoustic phonons. We use the Holland model exactly as described in the original work,[24] including the values of all fitting parameters, so it is not discussed further here. Below we describe our implementation of the Callaway model[23] with a modified umklapp scattering law as well as a BvKS model.[25]

The Callaway model is based on a Debye dispersion relation for a single, triply degenerate phonon branch. The Debye temperature $\theta_D = 530$ K is calculated from

$$\theta_D = (6\pi^2/V_P)^{1/3}\hbar v_s/k_B, \tag{A1}$$

where $V_P = 3.98 \times 10^{-29}$ m^3 (Ref. 55) is the volume of a primitive unit cell which contains two Si atoms and $v_s = 6084$ m/s (Ref. 33) is an average sound velocity. The original Callaway model[23] used an umklapp scattering rule with a lifetime proportional to T^{-3}, which is not appropriate for temperatures near or above the Debye temperature where the behavior is close to T^{-1}. Therefore, to adapt this model to high temperatures we replace Callaway's original umklapp scattering law with a common form,[27,45,56]

$$\tau_{PP}^{-1} = P\omega^2 T \exp\left(-\frac{C_U}{T}\right), \tag{A2}$$

where P and C_U are fitting parameters. For the natural silicon of interest in this work we neglect Callaway's k_2 correction term, which is only important for isotopically pure materials.[24,27,32] All other model parameters retain the same form as in the original paper.[23] We fit this modified Callaway model to the experimental data from Holland,[24] yielding the fitting parameters shown in Table V.

TABLE IV. Summary of thermal conductivity models used in this paper. A, b, C_U, and P_i are adjustable parameters.

Model	Dispersion	Phonon branch	Scattering rates: Boundary τ_B^{-1}	Scattering rates: Impurity τ_I^{-1}	Scattering rates: Phonon-phonon τ_{PP}^{-1}
Callaway (modified)	Debye	Average	v_g/b	$A\omega^4$	$P\omega^2 T e^{-C_U/T}$
Holland	Piecewise linear	$T0$	v_g/b	$A\omega^4$	$P_T\omega T^4$
		TU	v_g/b	$A\omega^4$	$P_{TU}\omega^2/\sinh(\frac{\hbar\omega}{k_B T})$
		L	v_g/b	$A\omega^4$	$P_L\omega^2 T^3$
BvKS	BvK	Average	v_g/b	$A\omega^4$	$P\omega^2 T e^{-C_U/T}$

The BvKS model is based on the Born–von Karman dispersion, $\omega = \omega_{\max}\sin(\pi q/2q_{\max})$, where $q_{\max} = 1.14 \times 10^{10}$ m^{-1} is the Debye cutoff wave vector based on the number density of primitive unit cells. The BvK dispersion includes the reduction of group velocity for wave vectors approaching the boundary of the first Brillouin zone,[25,33] although this rolloff is overestimated for LA modes in Si. As with our implementation of the Callaway model, in this BvKS model we approximate the three acoustic branches with a single effective branch based on an average sound velocity of 6084 m/s and use Eq. (A2) for phonon-phonon scattering. To the best of our knowledge this form of scattering time was first discussed by Slack,[56] which is the reason we refer to this model as BvKS.

APPENDIX B: ANALYTICAL ACCUMULATION FUNCTION FOR LONG MFP PHONONS

We present a convenient analytical form for the $\alpha(\Lambda_{\text{bulk}})$ function for phonons in the long MFP limit. This is a straightforward generalization of unpublished results for the case of ω^{-2} umklapp scattering recently obtained independently by Cahill[57] and then Freedman and Malen.[58] The form below should prove useful for extrapolating numerical accumulation functions such as from first-principles calculations,[20,47] which are unable to directly calculate very long MFPs, as well as interpreting measured accumulation functions.

We consider a general scattering power law,

$$\Lambda_{\text{bulk}} = A\omega^{-n}, \tag{B1}$$

where A may depend on T but not ω. This form applies for most common bulk scattering mechanisms, including impurities ($n = 4$), umklapp ($n = 2$), Akheiser damping[59] ($n = 0 - 2$), and boundaries ($n = 0$ or 1, Ref. 5). In a bulk sample usually $n > 0$, and thus large MFPs correspond to small ω, justifying a Debye approximation for the long-MFP tail regardless of T. Furthermore, for sufficiently small ω it is always true that $\hbar\omega << k_B T$, so it is convenient to approximate the Bose-Einstein function by $f \approx \frac{k_B T}{\hbar\omega}$. Focusing on a single scattering mechanism with $0 < n < 3$, applying this high-temperature Debye model to Eq. (2) yields

$$\kappa_{\text{bulk}} \propto \int_0^{\omega_D} \omega^{2-n} d\omega \propto \int_{\Lambda_D}^{\infty} \Lambda_{\text{bulk}}^{-\frac{3}{n}} d\Lambda_{\text{bulk}} \propto \Lambda^{1-\frac{3}{n}}\Big|_{\Lambda_D}^{\infty}, \tag{B2}$$

where $\Lambda_D = \Lambda_{\text{bulk}}(\omega_D)$ is the minimum MFP, e.g., at the Debye cutoff frequency. This form diverges for $n \geqslant 3$ in an infinite crystal, in which case we also allow for MFP truncation at some maximum length scale $L_{\max}$, much larger than Λ_D.

Continuing to the accumulation function $\alpha(\Lambda_{\text{bulk}})$ from Eq. (5), we consider four cases depending on the value of n. For $0 < n < 3$, as in umklapp scattering,

$$\alpha(\Lambda_{\text{bulk}}) = 1 - \left(\frac{\Lambda_{\text{bulk}}}{\Lambda_D}\right)^{1-\frac{3}{n}}. \tag{B3}$$

The analogous result for $n = 0$ is identical to the gray assumption discussed in the main text with $\Lambda_{\text{gr}} = \Lambda_D$, so the accumulation is a Heaviside step function, $H(\Lambda_{\text{bulk}} - \Lambda_D)$. Results for $n = 3$ and $n > 3$ are given in Table VI, where the last expression also assumes $L_{\max} \gg \Lambda_{\text{bulk}} \gg \Lambda_D$. We note that results equivalent to Eq. (B3) for $n = 2$ were obtained previously by Cahill[57] and Freedman and Malen.[58]

To apply these analytical forms to extrapolate the numerical results[20,47] of Fig. 6, we relax the derivation to require a pure power law only in the limit of small ω, while allowing arbitrary $\Lambda_{\text{bulk}}(\omega)$ for moderate and large ω. Thus, Eq. (B2) applies for all Λ_{bulk} beyond some threshold Λ_T defining the long tail regime, at which point the accumulation has the value $\alpha_T = \alpha(\Lambda_T)$. For example, this point (Λ_T, α_T) might be the longest MFP that was simulated numerically[20,47] or measured experimentally. For compactness we define a remainder function $r(\Lambda_{\text{bulk}}) = 1 - \alpha(\Lambda_{\text{bulk}})$ to describe the thermal conductivity contribution beyond Λ_{bulk}. Repeating the above analysis gives

$$r = r_T \cdot \left(\frac{\Lambda_{\text{bulk}}}{\Lambda_T}\right)^{1-\frac{3}{n}} \tag{B4}$$

TABLE V. Scattering parameters used in the Callaway and BvKS models.

	A (10^{-45} s^3)	P (10^{-19} sK^{-1})	C_U (K)	b (mm)
Callaway (modified)	2.73	2.73	173	5.7
BvKS	2.54	1.53	144	5.7

TABLE VI. Analytical forms for the accumulation functions in the high-temperature Debye limit corresponding to Eq. (B2) for different scattering exponents n.

	$n = 0$	$0 < n < 3$	$n = 3$	$n > 3$
$\alpha(\Lambda_{\text{bulk}}) =$	$H(\Lambda_{\text{bulk}} - \Lambda_D)$	$1 - \left(\frac{\Lambda_{\text{bulk}}}{\Lambda_D}\right)^{1-\frac{3}{n}}$	$\frac{\ln(\Lambda_{\text{bulk}}/\Lambda_D)}{\ln(L_{\max}/\Lambda_D)}$	$\frac{\Lambda_{\text{bulk}}^{1-\frac{3}{n}} - \Lambda_D^{1-\frac{3}{n}}}{L_{\max}^{1-\frac{3}{n}}}$

for $\Lambda_{\text{bulk}} \geqslant \Lambda_T$ and where $r_T = 1 - \alpha_T$. Recognizing that the point (Λ_T, r_T) is known, Eq. (B4) shows that the long MFP tail will still have a clean analytical form even though the behavior for $\Lambda_{\text{bulk}} < \Lambda_T$ may be much more complicated. Thus, if the power-law exponent in the long-MFP regime is believed to be known or bounded, Eq. (B4) should be useful for extrapolating an incomplete accumulation function.[20,47] Equation (B4) holds for $0 < n < 3$, while the analogous derivations for other values of n are similarly straightforward.

Equation (B4) also suggests convenient transformed axes for graphically identifying the dominant scattering exponent n from numerical and/or experimental data. In the long MFP (i.e., low-frequency) limit, a plot of $\ln(r)$ versus $\ln(\Lambda_{\text{bulk}})$ should be a straight line with slope $1 - \frac{3}{n}$, for MFP ranges where n is approximately constant and $0 < n < 3$. Figure 10 gives an example of these transformed axes. For Λ_T we choose the last available MFP from the 1stP calculation,[20,47] 6.58 μm, and anchor all curves to this point as indicated by the solid black circle. This calculation confirms that the long MFP tails of the Callaway,[23] Holland,[24] and BvKS[25,33] models all collapse onto the same $n = 2$ behavior, with a shape matching that obtained previously.[57,58] The MD results from Henry and Chen[14] have a slightly stronger exponent of $n \approx 2.1$ in this regime, while the 1stP results from Esfarjani *et al.*[20,47] are less clear but also appear to have n of around 2. Thus, the good agreement between all six curves of Fig. 10 in the long MFP regime confirms that Eqs. (B3) and (B4) should be a reliable basis for analytical extrapolation.

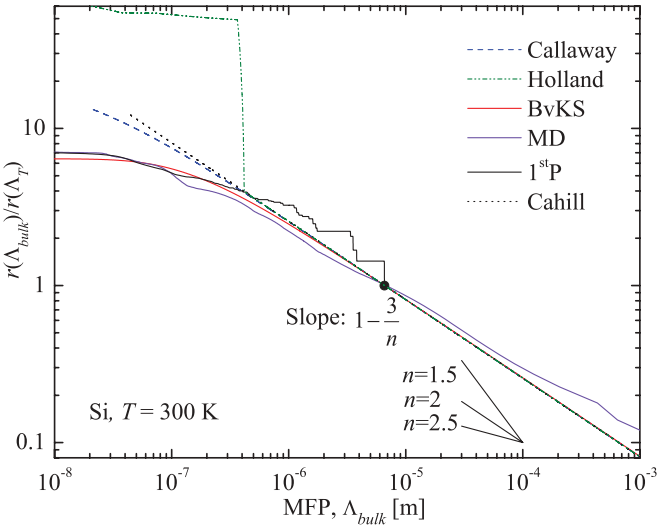

FIG. 10. (Color online) Remainder functions $r(\Lambda_{\text{bulk}}) = 1 - \alpha(\Lambda_{\text{bulk}})$ for different models in the long MFP region for Si at 300 K. All six curves are referenced to the same arbitrary tail point $\Lambda_T = 6.58$ μm.

*cdames@berkeley.edu

[1] D. Li, Y. Wu, P. Kim, L. Shi, P. Yang, and A. Majumdar, Appl. Phys. Lett. **83**, 2934 (2003).
[2] M. Asheghi, Y. K. Leung, S. S. Wong, and K. E. Goodson, Appl. Phys. Lett. **71**, 1798 (1997).
[3] W. Liu and M. Asheghi, J. Heat Transfer **128**, 75 (2006).
[4] D. Song and G. Chen, Appl. Phys. Lett. **84**, 687 (2004).
[5] Z. Wang, J. E. Alaniz, W. Jang, J. E. Garay, and C. Dames, Nano Lett. **11**, 2206 (2011).
[6] A. J. Minnich, M. S. Dresselhaus, Z. F. Ren, and G. Chen, Energy Environ. Sci. **2**, 466 (2009).
[7] J. Linan, W. Man, and Z. Yitshak, Meas. Sci. Technol. **10**, 653 (1999).
[8] Y. Cui, Q. Wei, H. Park, and C. M. Lieber, Science **293**, 1289 (2001).
[9] P. K. Schelling, L. Shi, and K. E. Goodson, Mater. Today **8**, 30 (2005).
[10] M. H. Huang, S. Mao, H. Feick, H. Yan, Y. Wu, H. Kind, E. Weber, R. Russo, and P. Yang, Science **292**, 1897 (2001).
[11] G. Chen, *Nanoscale Energy Transport and Conversion* (Oxford University Press, Oxford, 2005), p. 245.
[12] D. A. Broido, M. Malorny, G. Birner, M. Natalio, and D. A. Stewart, Appl. Phys. Lett. **91**, 231922 (2007).
[13] C. Dames and G. Chen, in *Thermoelectrics Handbook, Macro to Nano*, edited by D. M. Rowe (Taylor & Francis, New York, 2006).
[14] A. S. Henry and G. Chen, J. Comput. Theor. Nanosci. **5**, 141 (2008).
[15] C. Bera, N. Mingo, and S. Volz, Phys. Rev. Lett. **104**, 115502 (2010).
[16] D. P. Sellan, E. S. Landry, J. E. Turney, A. J. H. McGaughey, and C. H. Amon, Phys. Rev. B **81**, 214305 (2010).
[17] J. Garg, N. Bonini, B. Kozinsky, and N. Marzari, Phys. Rev. Lett. **106**, 045901 (2011).
[18] A. J. Minnich, J. A. Johnson, A. J. Schmidt, K. Esfarjani, M. S. Dresselhaus, K. A. Nelson, and G. Chen, Phys. Rev. Lett. **107**, 095901 (2011).
[19] Y. K. Koh and D. G. Cahill, Phys. Rev. B **76**, 075207 (2007).
[20] K. Esfarjani, G. Chen, and H. T. Stokes, Phys. Rev. B **84**, 085204 (2011).
[21] W. Li, N. Mingo, L. Lindsay, D. A. Broido, D. A. Stewart, and N. A. Katcho, Phys. Rev. B **85**, 195436 (2012).
[22] A. J. Minnich, Phys. Rev. Lett. **109**, 205901 (2012).
[23] J. Callaway, Phys. Rev. **113**, 1046 (1959).
[24] M. G. Holland, Phys. Rev. **132**, 2461 (1963).
[25] G. Chen, J. Heat Transfer **119**, 220 (1997).
[26] R. A. H. Hamilton and J. E. Parrott, Phys. Rev. **178**, 1284 (1969).
[27] M. Asen-Palmer, K. Bartkowski, E. Gmelin, M. Cardona, A. P. Zhernov, A. V. Inyushkin, A. Taldenkov, V. I. Ozhogin, K. M. Itoh, and E. E. Haller, Phys. Rev. B **56**, 9431 (1997).
[28] J. D. Chung, A. J. H. McGaughey, and M. Kaviany, J. Heat Transfer **126**, 376 (2004).
[29] C. Dames, *Micro/Nanoscale Heat Transfer International Conference* (National Cheng Kung University, Taiwan, 2008) (unpublished).
[30] N. Mingo and L. Yang, Phys. Rev. B **68**, 245406 (2003).
[31] R. Prasher, T. Tong, and A. Majumdar, Nano Lett. **8**, 99 (2007).
[32] N. Mingo, L. Yang, D. Li, and A. Majumdar, Nano Lett. **3**, 1713 (2003).

[33]C. Dames and G. Chen, J. Appl. Phys. **95**, 682 (2004).
[34]H. B. G. Casimir, Physica **5**, 495 (1938).
[35]A. K. McCurdy, H. J. Maris, and C. Elbaum, Phys. Rev. B **2**, 4077 (1970).
[36]R. B. Dingle, Proc. R. Soc. London A **201**, 545 (1950).
[37]K. Fuchs, Math. Proc. Cambridge Philos. Soc. **34**, 100 (1938).
[38]E. H. Sondheimer, Adv. Phys. **1**, 1 (1952).
[39]M. I. Flik and C. L. Tien, J. Heat Transfer **112**, 872 (1990).
[40]R. A. Richardson and F. Nori, Phys. Rev. B **48**, 15209 (1993).
[41]B. Poudel, Q. Hao, Y. Ma, Y. Lan, A. Minnich, B. Yu, X. Yan, D. Wang, A. Muto, D. Vashaee, X. Chen, J. Liu, M. S. Dresselhaus, G. Chen, and Z. Ren, Science **320**, 634 (2008).
[42]S. K. Bux, R. G. Blair, P. K. Gogna, H. Lee, G. Chen, M. S. Dresselhaus, R. B. Kaner, and J.-P. Fleurial, Adv. Funct. Mater. **19**, 2445 (2009).
[43]J. M. Ziman, *Electrons and Phonons: The Theory of Transport Phenomena in Solids* (Oxford University Press, Oxford, 1960), p. 463.
[44]J. S. Heron, T. Fournier, N. Mingo, and O. Bourgeois, Nano Lett. **9**, 1861 (2009).
[45]D. T. Morelli, J. P. Heremans, and G. A. Slack, Phys. Rev. B **66**, 195304 (2002).
[46]C. J. Glassbrenner and G. A. Slack, Phys. Rev. **134**, A1058 (1964).
[47]K. Esfarjani (private communication for 300 K data using the same method as Ref. 20).
[48]Y. S. Ju and K. E. Goodson, Appl. Phys. Lett. **74**, 3005 (1999).
[49]G. Chen, Phys. Rev. B **57**, 14958 (1998).
[50]A. I. Hochbaum, R. Chen, R. D. Delgado, W. Liang, E. C. Garnett, M. Najarian, A. Majumdar, and P. Yang, Nature (London) **451**, 163 (2008).
[51]A. I. Boukai, Y. Bunimovich, J. Tahir-Kheli, J.-K. Yu, W. A. Goddard Iii, and J. R. Heath, Nature (London) **451**, 168 (2008).
[52]J. Lim, K. Hippalgaonkar, S. C. Andrews, A. Majumdar, and P. Yang, Nano Lett. **12**, 2475 (2012).
[53]M. Asheghi, M. N. Touzelbaev, K. E. Goodson, Y. K. Leung, and S. S. Wong, J. Heat Transfer **120**, 30 (1998).
[54]W. H. Press, S. A. Teukolsky, W. T. Vetterling, and B. P. Flannery, *Numerical Recipes: The Art of Scientific Computing*, 3rd ed. (Cambridge University Press, Cambridge, 2007), p. 986.
[55]G. A. Slack, Phys. Rev. **105**, 829 (1957).
[56]G. A. Slack and S. Galginaitis, Phys. Rev. **133**, A253 (1964).
[57]D. G. Cahill (private communication).
[58]J. P. Freedman and J. A. Malen (private communication).
[59]B. C. Daly, K. Kang, Y. Wang, and D. G. Cahill, Phys. Rev. B **80**, 174112 (2009).